# ROMANSII: A TWO-DIMENSIONAL PROCESS SIMULATOR

C. D. Maldonado

Rockwell Semiconductor Products Division
Newport Beach, CA 92660, USA

## SUMMARY

A two-dimensional process simulator called ROMANSII† is discussed in this paper. The program is based on the numerical solution to the boundary-value problem which governs the redistribution of impurities during local oxidation of silicon (LOCOS). The formulations of this boundary-value problem in the physical domain of the device and in the transformed time-invariant rectangular domain, are presented. Default models for the concentration dependent diffusion coefficient and oxide growth which are integral parts of the boundary-value problem, are discussed together with the model used to specify the 2D distribution of an implant. The numerical procedure which involves a spatial discretization of the boundary-value problem in the stationary rectangular computational domain and use of Hindmarsh's GEARBI to solve the resultant stiff system of coupled nonlinear ordinary differential equations in the time as an initial-value problem, is briefly discussed. An application of ROMANSII to simulate the thermal redistribution of the n-well, field, channel, and source/drain implants through all the process steps of a standard 2 μm CMOS technology, is considered in detail. The results for the net impurity concentration of the final dopant profile were obtained as a function of vertical depth and lateral position along the width and length directions of both the n- and p-channel devices.

†ROMANS II (Redistribution and Oxidation Modeling ANalysis by Simulation in II-dimensions)

## 1. INTRODUCTION

During the past decade, the microelectronics industry has devoted considerable effort towards developing a mature VLSI technology. To achieve this objective, process and device simulators will play an important role in the design and fabrication of devices of small feature size. A search of the literature reveals that the development of two-dimensional (2D) device simulators is at a higher state than for process simulators. To eliminate this lag considerable research has recently been directed towards the development of 2D process simulators; however, the result of this effort has been simulators [1-4] for bulk device structures. In this paper a process simulator, ROMANSII, is presented which is capable of simulating the redistribution of impurities in bulk, as well as, SOS/SOI device structures.

The governing boundary-value problem for the redistribution of impurities during local oxidation of silicon is formulated in Sec. 2. Section 3 is devoted to a discussion of the default models for implant distribution, oxide growth, and concentration dependent diffusion coefficient. A brief discussion of the numerical procedure used to solve the boundary-value problem is presented in Sec. 4 since a more detail discussion is given elsewhere [5]. Finally, in Sec. 5 the program is used to simulate the redistribution of dopant profiles for a standard 2μm CMOS technology.

## 2. BOUNDARY-VALUE PROBLEM

The problem pertaining to the redistribution of impurities during LOCOS is important because other redistribution problems encountered in the fabrication of a device are special cases of it. To formulate the governing equations for this problem, the dynamically changing physical domain for a finite device structure as shown in Fig. 1(a) is utilized. In this figure the lateral dimension of the device cell, $|y| \leq B$, is assumed to repeat itself periodically in the lateral direction so that $y = 0$ and $\pm B$ are planes of symmetry. Without going into the details of the derivation it can be shown by conservation and continuity arguments together with the following assumptions:

- o there are no sinks or sources present in the physical domain
- o diffusion in oxide and substrate media is negligible
- o coupling of species is via the built-in electric field under the condition of local charge neutrality

that the governing boundary-value problem for the α specie is given as follows:

$$\frac{\partial}{\partial t} C_\alpha = \nabla \cdot \left[ \sum_\beta D_{\alpha\beta} \nabla C_\beta \right], \quad \{m\,U \le x \le L_o,\ 0 \le y \le B\}\ ; \tag{2.1}$$

$$\frac{\partial}{\partial y} C_\alpha \Big|_{y=0,B} = 0, \quad m\,U \le x \le L_o\ ; \tag{2.2}$$

$$\left.\begin{aligned} &\frac{\partial}{\partial x} C_\alpha \Big|_{x=L_o} = 0 \\ &\sum_\beta D_{\alpha\beta}\, \vec{n} \cdot \nabla C_\beta \Big|_{x=mU} = (k-m)\, \dot{U}_{\vec{n}}\, C_\alpha \Big|_{x=mU} \end{aligned}\right\}, \quad 0 \le y \le B\ ; \tag{2.3}$$

where the summation with respect to β is over all species. Symbols appearing in these equations and not defined in Fig. 1(a) are: k is the segregation coefficient; $U_n$ is the oxide growth rate normal to the $Si/SiO_2$ interface; $C_\alpha$ and $C_\beta$ are the total concentrations of the α and β species, respectively; and $D_{\alpha\beta}$ is the concentration dependent diffusion coefficient.

Besides being nonlinear the above boundary-value problem is further complicated by the complex and nonuniform movement of the $Si/SiO_2$ interface. No attempt was made to solve the

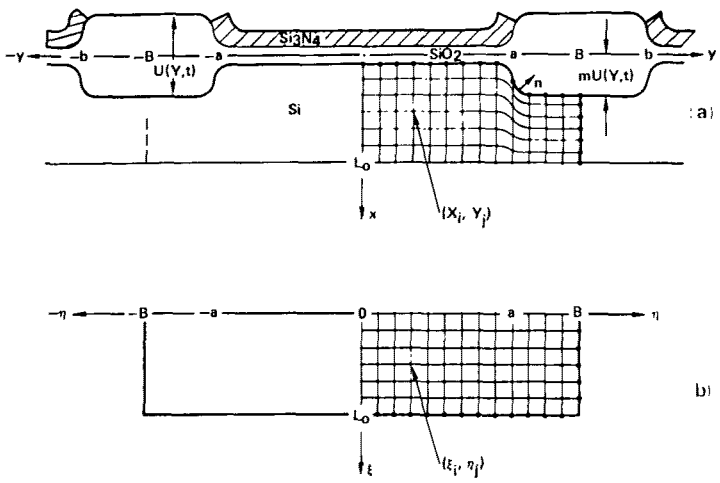


Fig. 1. Finite device structure during LOCOS and stationary rectangular computational domain in the transformed (ξ, η) coordinate system are shown in (a) and (b), respectively.

boundary-value problem in the physical domain of the device; instead, the procedure used was to transform the problem to a time-invariant rectangular computational domain like that shown in Fig. 1(b). To achieve this the following translation-scaling transformation:

$$\left.\begin{aligned} \xi &= \frac{[x-mU(y,t)]L_o}{L(y,t)} \\ \eta &= y \\ \tau &= t \end{aligned}\right\}, \tag{2.4}$$

where $L(y,t) = L_o - mU(y,t)$, is introduced. In a straight forward but tedious procedure, it can be shown that the above boundary-value problem given by (2.1 - 2.3) and defined on the shaded region, $\{mU \leq x \leq L_o,\ 0 \leq y \leq B\}$, of the physical domain of Fig. 1(a) can be transformed to the shaded region, $\{0 \leq \xi \leq L_o,\ 0 \leq \eta \leq B\}$, of the time-invariant rectangular domain of Fig. 1(b) as follows:

$$\begin{aligned} \frac{\partial}{\partial \tau} C_\alpha = \sum_\beta \{ & F_1(L,\xi,U_\eta) \frac{\partial}{\partial \xi}\left[D_{\alpha\beta} \frac{\partial}{\partial \xi} C_\beta\right] + \frac{\partial}{\partial \eta}\left[D_{\alpha\beta} \frac{\partial}{\partial \eta} C_\beta\right] \\ & - F_2(L,\xi,U_\eta) \left(\frac{\partial}{\partial \xi}\left[D_{\alpha\beta} \frac{\partial}{\partial \eta} C_\beta\right] + \frac{\partial}{\partial \eta}\left[D_{\alpha\beta} \frac{\partial}{\partial \xi} C_\beta\right]\right) \\ & + F_3(L,\xi,U_\tau,U_\eta,U_{\eta\eta},D_{\alpha\beta}) \frac{\partial}{\partial \xi} C_\beta\}, \\ & \{0 \leq \xi \leq L_o,\ 0 \leq \eta \leq B\}; \end{aligned} \tag{2.5}$$

$$- F_2(L,\xi,U_\eta) \frac{\partial}{\partial \xi} C_\alpha\Big|_{\eta=0,B} + \frac{\partial}{\partial \eta} C_\alpha\Big|_{\eta=0,B} = 0,\ 0 \leq \xi \leq L_o; \tag{2.6}$$

$$\left.\begin{aligned} & \frac{\partial}{\partial \xi} C_\alpha\Big|_{\xi=L_o} = 0 \\ & \sum_\beta \left\{F_4(L)D_{\alpha\beta} \frac{\partial}{\partial \xi} C_\beta - F_5(U_\eta) \frac{\partial}{\partial \xi} C_\beta\right\}\Big|_{\xi=0} \\ & \qquad = (k-m)U_\tau C_\alpha\Big|_{\xi=0} \end{aligned}\right\},\ 0 \leq \eta \leq B; \tag{2.7}$$

where

$$F_1(L,\xi,U_\eta) = \frac{L_o^2 + m^2 U_\eta^2 (L_o-\xi)^2}{L^2},$$

$$F_2(L, \xi, U_\eta) = \frac{mU_\eta(L_o - \xi)}{L} ,$$

$$F_3(L, \xi, U_\tau, U_\eta, U_{\eta\eta}, D_{\alpha\beta}) = \frac{m(L_o - \xi)}{L^2} \left[U_\tau L - (U_{\eta\eta} L + 2mU_\eta^2) D_{\alpha\beta}\right] ,$$

$$F_4(L) = \frac{L_o}{L} ,$$

and

$$F_5(U_\eta) = \frac{mU_\eta}{(1+m^2U_\eta^2)} .$$

If the substrate interface located at $\xi = L_o$ is allowed to recede to a remote position the above coefficients will reduce to the following:

$$F_1(L, \xi, U_\eta) \longrightarrow 1 + m^2U_\eta^2 ,$$

$$F_2(L, \xi, U_\eta) \longrightarrow mU_\eta ,$$

$$F_3(L, \xi, U_\tau, U_\eta, U_{\eta\eta}, D_{\alpha\beta}) \longrightarrow m[U_\tau - U_{\eta\eta} D_{\alpha\beta}] ,$$

$$F_4(L) \longrightarrow 1 ,$$

and $F_5(U_\eta)$ remains the same. With these coefficients (2.5 - 2.7) will then be the governing boundary-value problem for a bulk device structure.

## 3. DEFAULT MODELS

The default models used in ROMANSII to specify input information to the boundary-value problem for concentration dependent diffusion coefficient, oxide growth, and implant distribution, are discussed in this section.

### 3.1 Concentration Dependent Diffusion Coefficient

To be consistent with the derivation of the boundary-value problem which required the coupling of species to be via the built-in electric field under the condition of local charge neutrality, the concentration dependent diffusion coefficient is constrained to be of the following form:

$$D_{\alpha\beta} = \left[ D_\alpha + \frac{(kT/e)\mu_\alpha S_\alpha F_\alpha}{\sqrt{S^2 + 1}} \right] \delta_{\alpha\beta} +$$

$$\left[ \frac{Z_\beta (kT/e)\mu_\alpha S_\alpha F_\beta}{\sqrt{S^2 + 1}} \right] (1 - \delta_{\alpha\beta}) , \qquad (3.1)$$

where $\delta_{\alpha\beta}$ is the Kronecker symbol, i.e., $\delta_{\alpha\beta} = 1$ for $\alpha = \beta$ and 0 for $\alpha \neq \beta$; k is Boltzmann's constant; T is temperature; e is the electronic charge; $\mu_\alpha$ is the mobility of the $\alpha$ specie; $Z_\beta$ is + 1 when $\beta$ identifies a donor and -1 for an acceptor; $S_\alpha = f_\alpha(C_\alpha)/2n_i$; $n_i$ is the intrinsic carrier concentration; $f_\alpha(C_\alpha)$ is the electrically active concentration, $N_\alpha$, expressed as a specified function of the total concentration, $C_\alpha$;

$S = \sum_{\beta=1}^{M} Z_\beta (f_\beta(C_\beta)/2n_i)$ with M being the total number of coupled ionized donors and acceptors; $F_\alpha = \partial f_\alpha(C_\alpha)/\partial C_\alpha$; and $D_\alpha$ is that part of the concentration dependent diffusion coefficient which is responsible for diffusion via neutral and charged vacancy states.†† Assuming that an Einstein relation exists between $D_\alpha$ and $\mu_\alpha$, i.e. $D_\alpha = (kT/e)\ \mu_\alpha$, than (3.1) can be expressed as

$$D_{\alpha\beta} = \left\{ \left[ 1 + \frac{S_\alpha F_\alpha}{\sqrt{S^2 + 1}} \right] \delta_{\alpha\beta} + \left[ \frac{Z_\beta S_\alpha F_\beta}{\sqrt{S^2 + 1}} \right] (1-\delta_{\alpha\beta}) \right\} D_\alpha \qquad (3.2)$$

In the present version of ROMANSII, the following model [9]:

$$D_\alpha = \left\{ \frac{1 + \gamma_\alpha^+ (p/n_i) + \gamma_\alpha^- (n/n_i) + \gamma_\alpha^= (n/n_i)^2}{1 + \gamma_\alpha^+ + \gamma_\alpha^- + \gamma_\alpha^=} \right\} D_{\alpha i} \qquad (3.3)$$

which is applicable to boron, arsenic, and phosphorus, was chosen for $D_\alpha$. In this expression n and p are the electron and hole concentrations, respectively; $D_{\alpha i}$ is the intrinsic diffusion coefficient with the effects of oxidation enhanced diffusion (OED) incorporated; $\gamma_\alpha^+ = (D_\alpha^+/D_\alpha^\circ)$, $\gamma_\alpha^- = (D_\alpha^-/D_\alpha^\circ)$, and $\gamma_\alpha^= = (D_\alpha^=/D_\alpha^\circ)$ with $D_\alpha^\circ$, $D_\alpha^+$, $D_\alpha^-$, and $D_\alpha^=$ denoting the diffusivities of the neutral, singly charged

††Recent research [6-8] has shown that in order to properly account for oxidation enhanced diffusion (OED) in silicon, diffusion via interstitials is also required.

positive, singly charged negative, and doubly charged negative, vacancy states, respectively. For boron, arsenic, and phosphorus not all contributions from the various vacancy states are important and the following approximations to (3.3) are accurate models:

$$D_\alpha \left\{ \frac{1 + \gamma_\alpha^+ (p/n_i)}{1 + \gamma_\alpha^+} \right\} D_{\alpha i} \text{ (boron)} ,$$

$$D_\alpha \left\{ \frac{1 + \gamma_\alpha^- (n/n_i)}{1 + \gamma_\alpha^-} \right\} D_{\alpha i} \text{ (arsenic)} ,$$

and

$$D_\alpha \left\{ \frac{1 + \gamma_\alpha^- (n/n_i) + \gamma_\alpha^= (n/n_i)^2}{1 + \gamma_\alpha^- + \gamma_\alpha^=} \right\} D_{\alpha i} \text{ (phosphorus)} ,$$

where the normalized ratios $(n/n_i)$ and $(p/n_i)$ appearing in these equations can be expressed in terms of S as $S + \sqrt{S^2 + 1}$ and $-S + \sqrt{S^2 + 1}$, respectively.

## 3.2 Oxide Growth

Oxide growths frequently encountered in practice when certain prescribed initial oxide geometries are brought into contact with oxidizing ambients, are qualitatively shown in Fig. 2. To model these oxide growths the following phenomenological expression:

$$\tilde{U}(y,t) = \frac{[U(y,t) - U_o(y)]}{2} \operatorname{erfc} \left\{ \frac{(a-y) + \delta [U(t) - U_o]}{\sqrt{2}\, R_o U(t)} \right\} + U_o(y) \tag{3.4}$$

is utilized in ROMANSII, where

$$U(y,t) = -(\alpha/2) + [(\alpha/2)^2 + \beta t + \alpha U_o(y) + U_o^2(y)]^{1/2} , \tag{3.5}$$

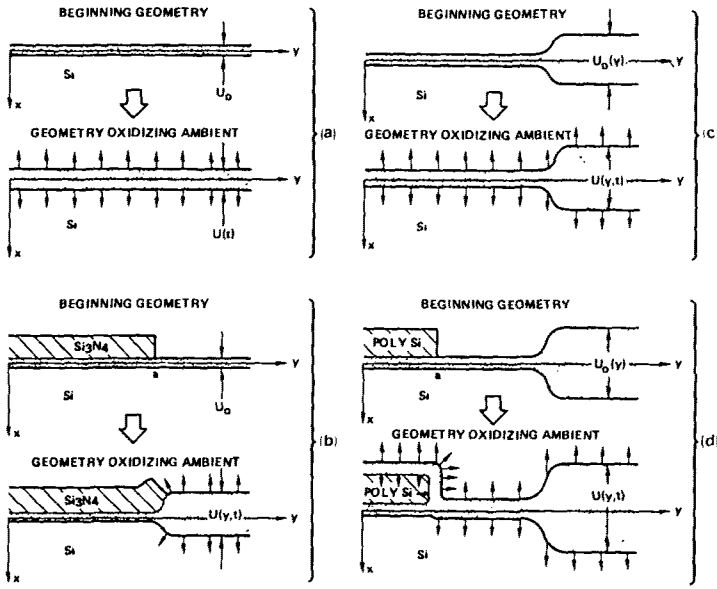


Fig. 2. Oxide growths frequently encountered in the fabrication of devices when various beginning oxide geometries are brought into contact with oxidizing ambients.

and*

$$U(t) = -(\alpha/2) + [(\alpha/2)^2 + \beta t + \alpha U_o + U_o^2]^{1/2}, \tag{3.6}$$

with (3.6) being the well-known expression of Deal-Grove [10]. The symbols appearing in these expressions are: a is the initial position of the nitride mask edge; $\delta$ is a factor which determines how much of the bird's beak region is under the nitride mask; $R_o$ is the ratio of lateral to vertical oxide growths and is a parameter which controls the lateral extend of the bird's beak region; $U_o(y)$ and $U_o$ are the specified initial nonuniform and uniform oxide thickness, respectively; and $\beta$ and $(\beta/\alpha)$ are respectively the parabolic and linear growth rate coefficients. Equation (3.4) which governs the situation shown in Fig. 2(d), will reduce to those for the other situations shown in Fig. 2. For example, the following are obtained: if the nitride's mask edge (y=a) is placed at a remote negative position far from the device cell then (3.4) will reduce to (3.5) which governs the situation shown in Fig. 2(c); if $U_o(y)$ is set equal to the uniform oxide pad under the nitride mask then (3.5) gives rise to

*Recently, a model [11] has been developed which eliminates the deficiency of (3.6) in predicting the growth of very thin oxides especially those grown in dry oxygen.

$$U(y,t) = \frac{[U(t) - U_o]}{2} \operatorname{erfc}\left\{\frac{(a-y) + \delta\,[U(t) - U_o]}{\sqrt{2}\,R_o U(t)}\right\} + U_o\ , \tag{3.7}$$

as the governing expression for the situation shown in Fig. 2(b); and finally, if $U_o(y)$ is set equal to an initial oxide of uniform thickness, $U_o$, and the nitride's mask edge (y=a) is placed at a remote negative position far from the device cell then (3.4) will reduce to (3.6) which governs the situation shown in Fig. 2(a).

## 3.3 Implant Distribution

The model of Runge [12] for calculating the 2D distribution of an implant after penetration through an effective mask whose cross-section varies arbitrarily with lateral position, is utilized. To be consistent with the formulation of Sec. 2 which assumes the device cell, $|y| \leq B$, is symmetric about y = 0 and repeats itself periodically in the lateral direction, the model of Runge is restricted in ROMANSII to effective mask geometries similar to that of Fig. 3(a). Using the property that the mask is symmetric about y = 0, the convolution integral of Runge for the implant distribution can then be expressed as:

$$C_{imp}(x,y) = \frac{C_d \cdot 10^4}{2\pi\sigma_p\sigma_L}\int_0^{+\infty} dy_o \left\{\exp\left[\frac{-(y-y_o)^2}{2\sigma_L^2}\right] + \exp\left[\frac{-(y+y_o)^2}{2\sigma_L^2}\right]\right\} \exp\left\{\frac{-[x+W(y_o)-X(y_o)-R_p]^2}{2\sigma_p^2}\right\}, \tag{3.8}$$

where $C_d$ is the dose; $W(y_o)$ is the thickness of the effective mask; $X(y_o)$ is the position of the $Si/SiO_2$ interface from the initial surface of the silicon wafer; $R_p$ is the projected range in silicon; and $\sigma_p$ and $\sigma_L$ are the vertical and lateral standard deviations, respectively.

The following expressions:

$$X(y_o) = m\,[U_{SiO_2}(y_o) + \sum_\rho U^e_{SiO_2,\rho}] \tag{3.9}$$

and

$$W(y_o) = U_{SiO_2}(y_o)\frac{R_p}{R_{p,SiO_2}} + \sum_\gamma U_\gamma(y_o)\frac{R_p}{R_{p,\gamma}}\ , \tag{3.10}$$

where the latter is based on the assumption of equivalent stopping powers, are used to calculate $X(y_o)$ and $W(y_o)$ as a

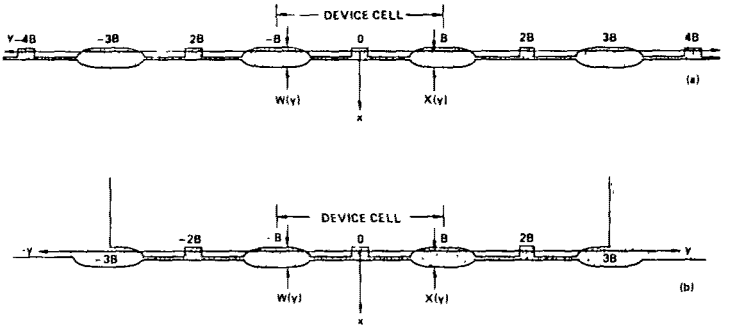


Fig. 3. Device cell ($|y| \leq B$) which repeats periodically in the lateral direction with an implant window over the entire structure ($|y| < \infty$) is illustrated in (a); while in (b) the window is closed for $3B \leq |y|$ by an impenetrable barrier.

function of lateral position. The first term on the right side of (3.10) is the contribution of the first $SiO_2$ layer adjacent to the silicon medium while the summation over $\gamma$ in the second term are the contributions of the subsequent layers. $U_{SiO_2}(y_o)$ and $U_\gamma(y_o)$ denote the physical thickness of these layers, and $R_{p,SiO_2}$ and $R_{p,\gamma}$ the projected range values. The term $\sum_\rho U^e_{SiO_2,\rho}$ in (3.9) is the accumulated thickness of all oxide uniformly etched from the first $SiO_2$ layer prior to the introduction of the implant.

To evaluate the above integral the window opening for the implant which is over the entire periodic structure of Fig. 3(a), was restricted to the device cell and adjacent neighboring cells as shown in Fig. 3(b) where in the region $|y| \geq 3B$, the mask is taken as an impenetrable barrier to the implant. For this latter mask geometry (3.8) reduces to

$$C_{imp}(x,y) = \frac{C_d \cdot 10^4}{2(2\pi)^{1/2}\sigma_p} \left\{ F^+_{0\to 3B}(x,y) + F^-_{0\to 3B}(x,y) \right\} , \quad (3.11)$$

where

$$F^{\pm}_{0\to 3B}(x,y) = \frac{1}{\sigma_L} \left(\frac{2}{\pi}\right)^{1/2} \int_0^{3B} dy_o \exp\left[\frac{-(y\pm y_o)^2}{2\sigma_L^2}\right]$$

$$\exp\left\{\frac{-[x+W(y_o)-X(y_o)-R_p]^2}{2\sigma_p^2}\right\} . \quad (3.12)$$

The analytical procedure for evaluating the integrals of (3.12) involves approximating both $W(y_o)$ and $X(y_o)$ by straight line segments as follows: $W(y_o) = W_i + A_i(y-y_{oi})$ and $X(y_o) = X_i + B_i(y-y_{oi})$ for $y_{oi} \leq y_o \leq y_{oi+1}$, where $y_{o1}, y_{o2}, \ldots, y_{oi}, \ldots, y_{oM}$ are the lateral positions of the grid points used to solve the boundary-value problem of Sec. 2. In terms of $W_i = W(y_{oi})$, $W_{i+1} = W(y_{oi+1})$, $X_i = X(y_{oi})$, and $X_{i+1} = X(y_{oi+1})$ which are specified through (3.9) and (3.10), the slopes are calculated as $A_i = (W_{i+1} - W_i)/d_i$ and $B_i = (X_{i+1} - X_i)/d_i$, where $d_i = y_{oi+1} - y_{oi}$. The result of this procedure is

$$F^{\pm}_{0\to 3B}(x,y) = \sum_{i=1}^{M-1} C_i \exp\left[-D_i^{\pm}(x,y,y_{oi})\right] \cdot \left(\operatorname{erf}\{E_i[y_{oi+1} + G_i^{\pm}(x,y,y_{oi})]\} - \operatorname{erf}\{E_i[y_{oi} + G_i^{\pm}(x,y,y_{oi})]\}\right) , \tag{3.13}$$

where

$$C_i = \left[1 + (A_i - B_i)^2 R^2\right]^{-1/2} ,$$

$$D_i^{\pm}(x,y,y_{oi}) = \frac{\left[H_i(x,y_{oi}) \pm (B_i - A_i)y\right]^2 C_i^2}{2\sigma_p^2} ,$$

$$E_i = \frac{1}{\sqrt{2}\sigma_L C_i} ,$$

$$G_i^{\pm}(x,y,y_{oi}) = \left[(A_i - B_i)\, H_i(x,y_{oi})\, R^2 \pm y\right] C_i^2 ,$$

$$H_i(x,y_{oi}) = x + (W_i - X_i) - (A_i - B_i)y_{oi} - R_p ,$$

and

$$R = \frac{\sigma_L}{\sigma_p} .$$

For most applications involving devices with feature size as small as two microns the upper limit of 3B in the integral of (3.12) was adequate; because as this limit was changed from 3B to 5B, 7B, etc. to include contributions from additional neighboring cells the observed change on the implant profile in the physical domain of the device was insignificant.

## 4. NUMERICAL PROCEDURE

In the present version of ROMANSII the coupling of species is neglected, i.e., the terms in the summation over $\beta$ in the transformed boundary-value problem given by (2.5 - 2.7) for which $\beta \neq \alpha$ are not considered. The numerical solution to the resultant boundary-value problem is briefly discussed in this section because a more detailed discussion is given elsewhere [5]. The rectangular computational domain of Fig. 1(b) was subdivided into a uniform grid with coordinates $(\xi_i, \eta_j)$ using meshwidths $\Delta\xi = \xi_{i+1} - \xi_i$ and $\Delta\eta = \eta_{i+1} - \eta_i$. This gave rise to $N_\xi = (L_o/\Delta\xi) + 1$ and $N_\eta = (B/\Delta\eta) + 1$ grid points in the vertical and lateral directions, respectively. On this uniform grid a straight forward procedure employing centered difference approximations was used to discretize the spatial derivations of (2.5 - 2.7). The results of this procedure was a semidiscrete system,

$$\frac{d}{d\tau} C_{ij} = f(C_{ij}, C_{i-1,j}, C_{i+1,j}, C_{i,j+1}, C_{i,j-1}, C_{i+1,j+1}, C_{i-1,j+1}, C_{i+1,j-1}, C_{i-1,j-1}, \tau) \tag{4.1}$$

of $N_\xi \times N_\eta$ coupled ordinary nonlinear differential equations in the time domain. This stiff system of equations was solved as an initial-value problem for an arbitrarily specified initial distribution, $C_{ij}(\tau=0)$. The solution was obtained by the variable-order and variable-step-size stiff integrator of Hindmarsh [13], which is optimally first to fifth order accurate in the time variable. Because of the uniform centered differencing in the spatial directions, the difference operators in this procedure are second order accurate in $\xi$ and $\eta$. The strong point of this procedure is the excellent error control of the integrator which allows both the time step and order of integration to be selected in an optimal manner. Finally, it should be noted that the solution obtained by this numerical procedure was the base on which ROMANSII was developed.

## 5. APPLICATION

In this section the redistribution of the dopant profiles for the 2 μm CMOS technology [14] shown in Fig. 4, is considered. This technology employs eight mask operations including a passivation mask and uses a LOCOS scheme for device isolation. A brief description of the process steps is now presented. Using a LPCVD nitride and CVD oxide layer as mask, the n-well phosphorus implant is performed. This is followed by a high temperature drive step to form the well. The active layer is then delineated, and the CVD oxide, nitride and thin thermal oxide layers are dry etched so as to expose the field areas of both p- and n-channel devices. This is followed by a

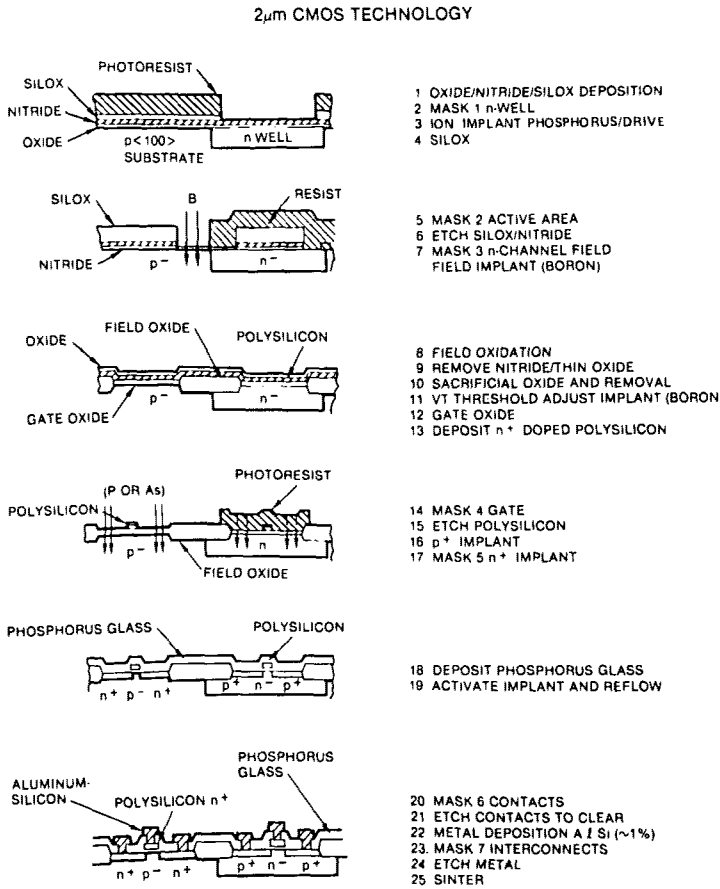


Fig. 4. Process schedule for a standard 2μm CMOS technology.

field implant for the n-channel field threshold voltage enhancement using the thick CVD oxide as mask. The field oxidation step is performed at this point after removing the top CVD oxide from the active regions. This is followed by the growth and removal of the sacrificial oxide. The gate oxide is then grown and a threshold voltage adjust implant (boron) is introduced into the channel regions. Polysilicon ($n^+$) and molybdenum silicide gates are deposited and patterned, followed by source/drain implantation for both p- and n-channel devices. Next, a phosphorus doped crossover oxide is deposited, and the contacts are delineated and etched. Following the activation of the source/drain implants and reflow cycle for improving step coverage, an aluminum silicon metal layer is deposited. The interconnects are patterned and etched, and wafers are sintered. A passivation layer deposition and opening of pads completes the fabrication process.

ROMANSII was used to simulate the thermal redistribution of the phosphorus, boron, and arsenic impurities through all the process steps of Fig. 4. These simulations were carried out along the width and length directions of the n- and p-channel devices. The top view which is applicable to both device, and cuts along which the simulations were carried out, are qualitatively shown in Fig. 5. A ROMANSII input format which is similar to that of the SUPREM program but modified to handle 2D problems, was used to code these redistribution problems. Model parameters for the key process steps (oxidation/drive-in, implantation, etch, and deposition), were generated using subroutines of the SUPREMII program [15]. Because SUPREMII is a one-dimensional program, the stored data for the projected range statistics was extended to include information on the lateral standard deviation using the same data source [16]. The parameters $R_o$ and $\delta$ of the LOCOS process step were obtained by requiring the simulated cross-sectional view of the bird's beak region to be consistent with SEM data. The effects of clustering which become important at high impurity concentrations, are taken into account through the de-enhancement factor, $F_\alpha = \partial f_\alpha(C_\alpha)/\partial C_\alpha$, in the diffusion coefficient of (3.2). A subroutine based on the model used in SUPREMII to relate the total concentration to the electrically active impurity concentration, has been incorporated into ROMANSII to evaluate $F_\alpha$.

The simulated results along the width and length directions of the n-channel device are shown in Figs. 6 and 7, respectively, while the corresponding results for the

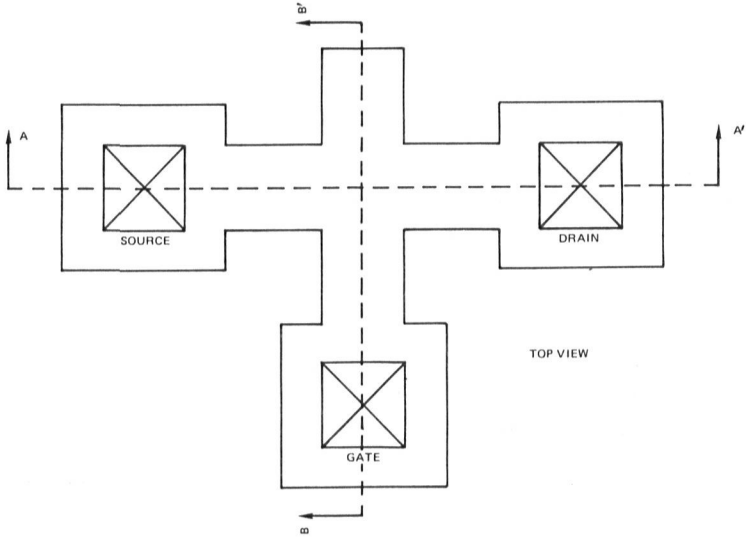


Fig. 5. Top view for p- and n-channel devices with cuts AA' (length direction) and BB' (width direction) along which ROMANSII simulations were carried out.

p-channel device are shown in Figs. 8 and 9. In each figure the surface topography and corresponding equi-density contours for the final net dopant profile are plotted as a function of vertical depth and lateral position. Because y=0 is a plane of symmetry the net dopant profile is plotted only to the right of this plane. The results in Fig. 6 for the n-channel device reveal the usual and unavoidable encroachment of both the field oxide and boron profile into the channel region. The results of Fig. 7 are similar to those of Fig. 6 except that a heavily doped source/drain region of arsenic has been inserted between the channel and field regions. This heavily doped ($\sim 1.4 \times 10^{20}$ $cm^{-3}$) source/drain region is characterized by a junction depth of 0.25 μm and lateral penetration under the polysilicon gate of 0.17 μm. An examination of the results of Fig. 8 for the p-channel device reveals the same encroachment of the field oxide into the channel region but they

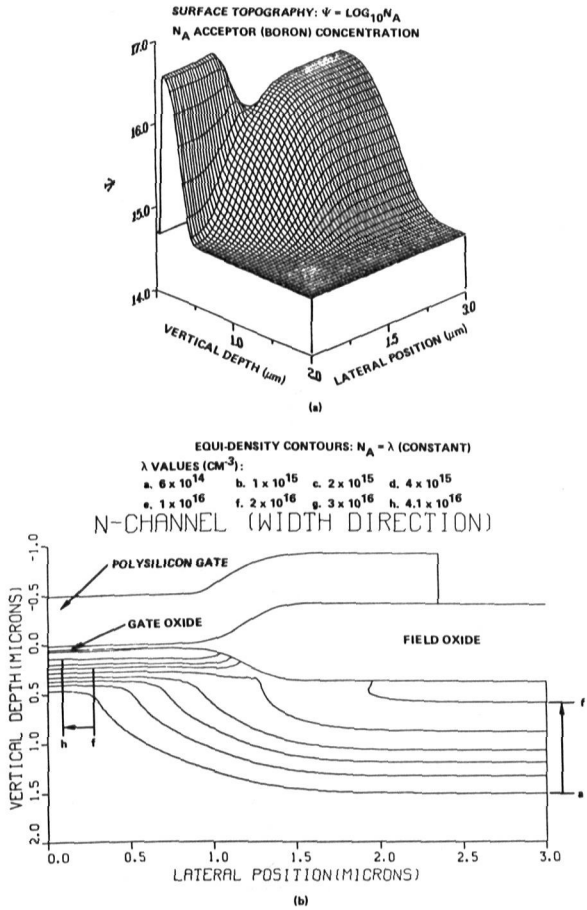


Fig. 6. Surface topography and corresponding equi-density contours along the width direction of the n-channel device.

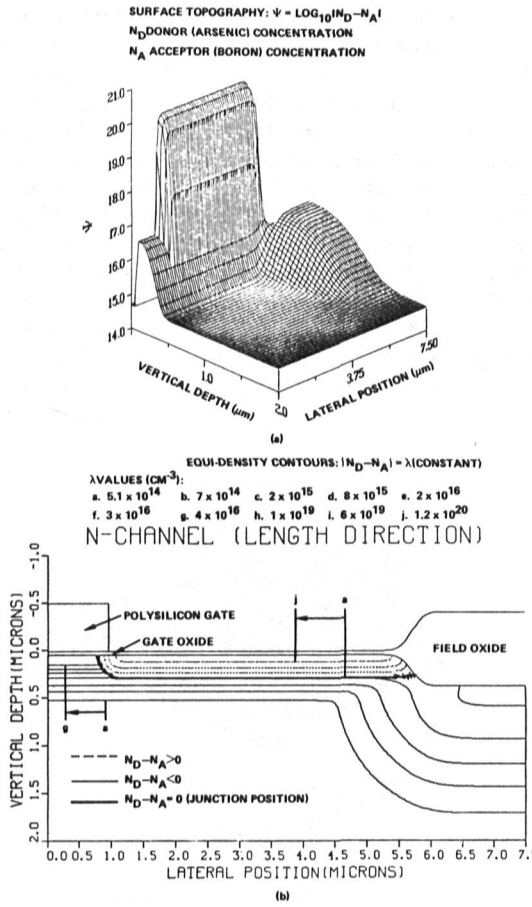


Fig. 7. Surface topography and corresponding equi-density contours along the length direction of the n-channel device.

differ from those of Fig. 6 in the following way: a junction located 0.22 μm from the $Si/SiO_2$ interface exists such that in the lightly doped layer which is bounded by the junction and $Si/SiO_2$ interface, the redistributed boron threshold voltage adjust implant is dominant over the redistributed phosphorous n-well implant while in the region on the other side of the junction the converse is true. In Fig. 9 a heavily doped ($\sim 4 \times 10^{19}$ $cm^{-3}$) source/drain region of boron has been introduced between the channel and field regions; otherwise, the results of this figure are similar to those of Fig. 8. The junction depth and lateral penetration under the polysilicon gate of the heavily doped boron source/drain region are 0.42 μm and 0.27 μm, respectively. Finally, it should be noted that the results of Figs. 6 to 9 correlated well with those obtained by SUPREMII along cuts where the net dopant profile is essentially one dimensional. Also, it was shown in Ref. 15 that a

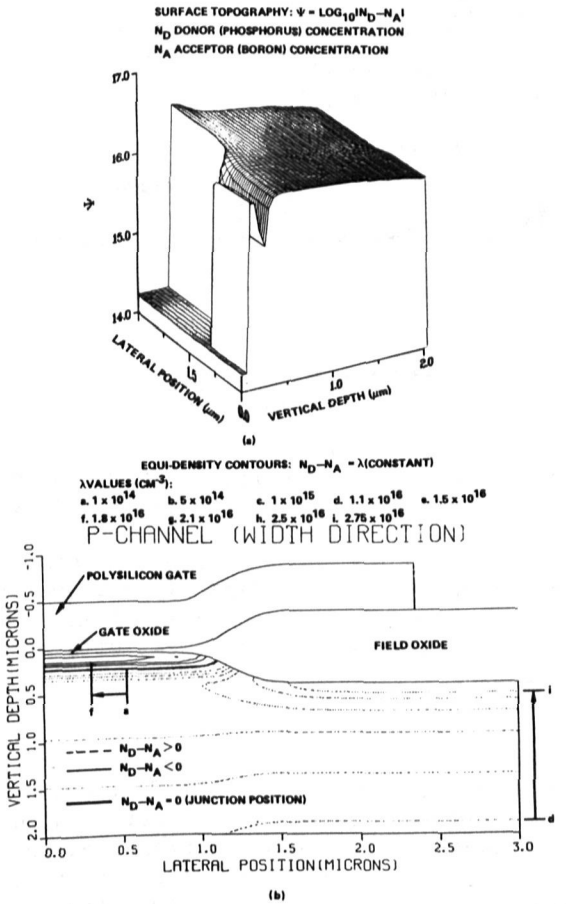


Fig. 8. Surface topography and corresponding equi-density contours along the width direction of the p-channel device.

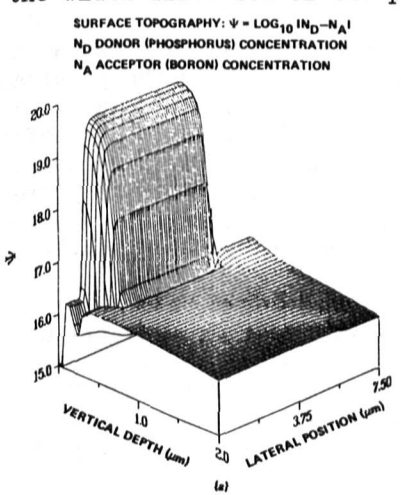

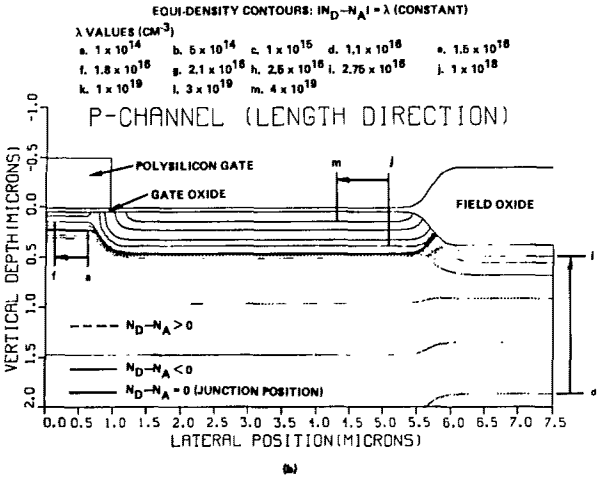


(b)

Fig. 5. Surface topography and corresponding equi-density contours along the length device of the p-channel device.

boron profile similar to that of Fig. 6 but obtained under slightly different conditions by ROMANSII, yielded one-dimensional distributions deep in the channel and field regions that were in satisfactory agreement with those obtained by spreading resistance measurements.

## 6. CONCLUSION

The two-dimensional simulator, ROMANSII, which is capable of predicting the redistribution of impurities in bulk and finite (SOS/SOI) device structures, is presented in this paper. This simulator is based on the solution to the most general boundary-value problem which governs the redistribution of high concentration impurities during LOCOS. Because of the complex and nonuniform movement of the $Si/SiO_2$ interface, the boundary-value problem was not solved in the physical domain of the device. Instead, a translation-scaling transformation was used to transform the physical domain of the device to a fixed time-invariant rectangular computational domain. In the computational domain the transformed boundary-value problem with the coupling of species neglected, was spatially discretized and the resultant stiff system of coupled ordinary nonlinear differential equations was solved as an initial value problem using the best currently available integrator, GEARBI.

Simulations to investigate the redistribution of the n-well, field, channel, and source/drain implants which are used in the fabrication of a standard 2μm CMOS technology, were carried out using ROMANSII. The results for the net impurity concentration of the final dopant profile were

obtained as a function of vertical depth and lateral position along the width and length directions of both the n- and p-channel devices. These results represent the first complete two-dimensional description of the final dopant profile as it exists in a standard CMOS device structure.

## ACKNOWLEDGMENT

The author would like to thank W. D. Murphy and W. F. Hall of the Rockwell Science Center who were responsible for obtaining the numerical solution to the nonlinear boundary-value problem; S. A. Louie who provided the scientific programming support and worked so hard to make ROMANSII a practical 2D process simulator; and F. Z. Custode who kindly provided the 2μm CMOS technology used in this paper.

## REFERENCES

1. D. J. Chin, M. K. Kump, H. G. Lee, and R. W. Dutton, "Process Design Using Two-Dimensional Process and Device Simulators," IEEE Trans. Electron Devices, Vol. ED-29, p. 336, 1982.

2. K. Taniguchi, M. Kashiwagi, and H. Iwai, "Two-Dimensional Computer Simulation Models for MOSLSI Fabrication Processes," IEEE Trans. Electron Devices, Vol. ED-28, p. 574, 1981.

3. R. Tielert, "Two-Dimensional Numerical Analysis of Doping Processes," Proc. NASECODEIII B. T. Browne and J. J. H. Miller, Eds. Boole Press, Dublin, Ireland, 1983.

4. B. R. Penumali, "Lateral Oxidation and Redistribution of Dopants," Proc. NASECODEII, B. T. Browne and J. J. H. Miller, Eds. Boole Press, Dublin, Ireland, 1981.

5. W. D. Murphy, W. F. Hall, C. D. Maldonado, and S. A. Louie, "MEMBRE: An Efficient Two-Dimensional Process Code for VLSI," COMPEL, Vol. 1, p. 219, 1983.

6. A. M. Lin, D. A. Autoniadis, and R. W. Dutton, "The Oxidation Rate Dependence of Oxidation-Enhanced Diffusion of Boron and Phosphorous in Silicon," J. Electrochem. Soc., Vol. 128, p. 1131, 1981.

7. T. Y. Tan, U. Gösele, and F. F. Morehead, "On the Nature of Point Defects and the Effect of Oxidation on Substitutional Dopant Diffusion in Silicon," Appl. Phys., Vol. A31, p. 97, 1983.

8. C. P. Ho, J. D. Plummer, S. E. Hansen, and R. W. Dutton, "VLSI Process Modeling - SUPREMIII," IEEE Trans. Electron Devices, Vol. ED-30, p. 1438, 1983.

9. R. B. Fair, "Concentration Profiles of Diffused Dopants in Silicon," In: Impurity Doping Process in Silicon (Ed. F. F. Y. Want), North-Holland, Amsterdam, The Netherlands, in press.

10. B. E. Deal and A. S. Grove, "General Relationship for the Thermal Oxidation of Silicon," J. Appl. Phys., Vol. 36, p. 3770, 1965.

11. H. Z. Massoud, "Growth Kinetics of Thin $SiO_2$ Layers in Dry Oxygen," In: Computer-Aided Design of IC Fabrication Processes (Ed. J. D. Plummer), Stanford Electronics Laboratories, Stanford University, Stanford, CA, Tech. Rep., July 1982.

12. H. Runge, "Distribution of Implanted Ions Under Arbitrarily Shaped Masked Edges," Phys. Status. Solidi, Vol. (a) 39, p. 595, 1977.

13. A. C. Hindmarsh, "Preliminary Documentation of GEARBI: Solution of ODE Systems with Block-Iterative Treatment of the Jacobian," Lawrence Livermore Laboratory Report UCID-30149, Livermore, CA, 1976.

14. C. D. Maldonado, F. Z. Custode, S. A. Louie, and R. K. Pancholy, "Two-Dimensional Simulation of a 2-μm CMOS Process Using ROMANSII," IEEE Trans. Electron Devices, Vol. ED-30, p. 1462, 1983.

15. D. A. Antoniadis, S. E. Hansen, and R. W. Dutton, "SUPREMII - A Program for IC Process Modeling and Simulation," Stanford Electronic Lab., Tech. Rep. 5019-2, June 1978.

16. J. F. Gibbons, W. S. Johnson, and S. Mylroie, "Projected Range Statistics" Dowden, Hutchinson, and Ross, Stroudsbourgh, PA, 1975.